Effect of insulin insufficiency on ultrastructure and function in skeletal muscle

Chantal Kopecky[1], Michael Haug[2], Barbara Reischl[2], Nandan Deshpande[3], Bikash Manandhar[1], Thomas W. King[1], Victoria Lee[1], Marc R Wilkins[4, 5], Margaret Morris[1], Patsie Polly[1], Oliver Friedrich[1,2], Kerry-Anne Rye[1]*, Blake J Cochran[1]*

[1] School of Biomedical Sciences, Faculty of Medicine & Health, UNSW Sydney, Sydney, Australia

[2] Institute of Medical Biotechnology, Department of Chemical and Biological Engineering, Friedrich-Alexander University Erlangen-Nürnberg, Erlangen, Germany

[3] Sydney Informatics Hub, University of Sydney, Sydney, Australia

[4] Systems Biology Initiative, Faculty of Science, UNSW Sydney, Sydney, Australia

[5] Ramaciotti Centre for Genomics, UNSW Sydney, Sydney, Australia

* These authors contributed equally.

Correspondence:

Blake Cochran, School of Biomedical Sciences, UNSW Sydney. Email: b.cochran@unsw.edu.au

Kerry-Anne Rye, School of Biomedical Sciences, UNSW Sydney. Email: k.rye@unsw.edu.au

Abstract

Background: Decreased insulin availability and high blood glucose levels, the hallmark features of poorly controlled diabetes, drive disease progression and are associated with decreased skeletal muscle mass. We have shown that mice with β-cell dysfunction and normal insulin sensitivity have decreased skeletal muscle mass. This project asks how insulin deficiency impacts on the structure and function of the remaining skeletal muscle in these animals.

Methods: Skeletal muscle function was determined by measuring exercise capacity and specific muscle strength prior to and after insulin supplementation for 28 days in 12-week-old mice with conditional β-cell deletion of the ATP binding cassette transporters ABCA1 and ABCG1 (β-DKO mice). *Abca1* and *Abcg1* floxed (fl/fl) mice were used as controls. Expression of genes encoding for skeletal muscle atrophy markers and signaling pathways were quantified by RNA-seq expression profiling. Skeletal muscle and mitochondrial morphology were assessed by transmission electron microscopy. Sarcomere patterns were assessed by label-free Second Harmonic Generation microscopy. Myofibrillar Ca^{2+} sensitivity and maximum isometric single muscle fibre force were assessed using *MyoRobot* biomechatronics technology.

Results: 59 RNA transcripts involved in muscle contraction and movement were significantly altered in β-DKO mice compared to fl/fl controls. Exercise capacity and muscle strength were significantly decreased in β-DKO mice compared to fl/fl controls (p=0.012), and a loss of structural integrity was also observed in skeletal muscle from the β-DKO mice. Supplementation of β-DKO mice with insulin restored muscle integrity, strength and expression of 21 of the dysregulated transcripts.

Conclusions: Insulin insufficiency due to β-cell dysfunction perturbs the structure and function of skeletal muscle. These adverse effects are rectified by insulin supplementation.

Keywords: Insulin, skeletal muscle, muscle structure, muscle function

Introduction

Skeletal muscle wasting and weakness (sarcopenia) are serious pathological complications of aging and disease[1]. Sarcopenia is a predictor of poor disease outcomes in diabetes[2], cancer[3], chronic heart failure[4] and pneumonia[5] as well as in subjects without underlying disease[6]. A major contributing factor to muscle atrophy is a reduction in circulating levels of the anabolic hormone insulin to below the required threshold for maintaining glucose and muscle homeostasis[1], either due to insulin resistance or some other insulinopenia.

Beyond the use of exogenous insulin, current treatments for muscle atrophy in diabetes are limited to diet, exercise and the use of insulin sensitising medications such as metformin. However, these options only partially mitigate muscle loss[7]. Whilst impaired muscle metabolism is acknowledged as a serious problem in people with diabetes, questions remain as to the underlying molecular mechanisms that are responsible for this dysfunction and associated structural changes. Moreover, it remains unclear if skeletal muscle dysfunction is a cause or consequence of insulin resistance and disease progression.

Skeletal muscle, which is the main site of glucose disposal, plays a critical role in maintaining glycaemic control[8, 9]. Impaired skeletal muscle metabolism and significant loss of muscle mass due to increased breakdown of myofibrillar proteins, together with reduced exercise capacity, are common in patients with diabetes[10]. Muscle atrophy due to an imbalance in contractile protein synthesis and degradation is also triggered by diabetes[11]. However, there is also evidence that muscle atrophy in diabetes is primarily driven by decreased protein synthesis rather than increased proteolysis[12].

Characterisation of the molecular mechanism(s) by which insufficient insulin action disrupts muscle homeostasis *in vivo* is complicated by limitations in currently available animal

models. The most common mouse models of diabetes, the *db/db* mouse and the diet induced obesity (DIO) mouse are primarily models of insulin resistance, with secondary compensatory hyperinsulinemia that exceeds physiological levels found in humans. Chemical destruction of pancreatic β-cells in rats and mice with streptozotocin and muscle-specific deletion of the insulin receptor in mice have provided useful insights, but these are models of a total absence of insulin action. Mice with decreased insulin gene dosage have decreased muscle mass[13] and no change in strength[14], but the transcriptional and functional implications of this genetic deletion are not understood, and it is not known if restoration of circulating insulin levels can reverse this phenotype.

We have previously described a mouse model of pancreatic β-cell dysfunction due to conditional deletion of the cholesterol transporters, ABCA1 and ABCG1 (β-DKO mice)[15]. These mice have approximately half of the circulating insulin levels of littermate fl/fl controls[15]. They also lack the first phase of insulin secretion in response to glucose but have normal insulin sensitivity and have markedly decreased skeletal muscle mass and increased fat mass due to a shift in glucose disposal from muscle to adipose tissue, which can be normalised by supplementation with insulin[15].

This study investigates the consequences of the loss of muscle mass in these mice by asking whether the structure and function of the remaining skeletal muscle is impaired. We investigated the direct effects of insulin insufficiency in the animals by quantifying changes in skeletal muscle gene transcription and morphology, as well as exercise capacity and muscle strength. Evidence that insulin supplementation partly restores skeletal muscle homeostasis in these mice is also presented.

Materials and Methods

Animal studies

β-DKO and fl/fl control mice were generated as described previously[15]. All experiments were performed on 12-week-old male mice. The animals were maintained on a standard chow diet in a specific pathogen-free laboratory with a 12 h light/dark cycle. All animal experiments were approved by the Animal Ethics Committee, UNSW Sydney, Ethics Number 16/167B.

Insulin supplementation

β-DKO mice were supplemented with insulin or PBS (control) in mini-osmotic pumps (Model 1004, Alzet, Cupertino, CA) as described previously[15]. Fl/fl littermate control mice received pumps containing PBS. The pumps were loaded with Humulin R (0.1 U/day, Eli Lily, Indianapolis, IN) or an equivalent volume of PBS prior to subcutaneous implantation between the shoulder blades of anesthetized mice The mice were euthanized by cervical dislocation 28 days post-pump implantation.

Tissue collection

The *extensor digitorum longus* (EDL) muscle was rapidly excised after euthanasia and either used for biomechanics experiments, fixed overnight at 4 °C for microscopy experiments or snap-frozen in liquid nitrogen and stored at -80 °C until further use.

Gene expression studies

Total RNA was extracted from EDL muscle using an miRNeasy mini kit (Qiagen, Venlo, Netherlands) according to the manufacturer's protocol. Samples from three separate animals were pooled to ensure RNA was of sufficient quantity and quality for analysis. RNA was analysed for quality and integrity and sequenced using Agilent 2100 Bioanalyzer

(Agilent Technologies, Santa Clara, CA). Libraries were prepared from 500 ng of total RNA/sample using TruSeq Stranded mRNA-seq prep. Each library was single-read sequenced (1×75 bp) using NextSeq 500 High Output flow cell (60 million reads per sample).

Bioinformatic analysis

RNA-seq reads were first assessed for quality using the FastQC tool (v0.11.8) (www.bioinformatics.babraham.ac.uk/projects/fastqc/). The tool Salmon was used for quantifying transcript abundance from RNA-seq reads[16]. A mouse transcriptome which contained the super-set of all transcripts coding sequences resulting from Ensembl gene predictions (Mus musculus.GRCm38) was downloaded and converted into a Salmon index file (ftp://ftp.ensembl.org/pub/release-101/fasta/mus_musculus/cds/). This index file was used as a reference file for the mapping and quantification step. Transcript level quantifications were converted to gene level quantifications for downstream differential expression analysis.

Differentially expressed genes across all of the conditions were identified using the Bioconductor package edgeR v3.28.0 in the R programming environment[17]. Read counts were normalised using the between lane normalisation of EDASeq with upper quartile normalisation[18]. The R package, RUV, of Risso et al. was used to remove unwanted variation caused by batch effects using empirical control genes[19]. Differentially expressed genes identified with a false discovery rate (FDR) <0.1 cut-off were considered to be significantly upregulated or downregulated. The Mouse Portal within the Rat Genome Database[20] was used to identify canonical pathways associated with the differentially expressed genes.

EchoMRI

The percentage of body fat and lean tissue mass of the animals was determined using an EchoMRI-900 Body Composition Analyzer (Biological Resources Imaging Laboratory, UNSW Sydney). Body fat percentage was calculated as:

$$\frac{fat\ mass}{(fat\ mass + lean\ mass)} \times 100$$

and lean mass percentage as:

$$\frac{lean\ mass}{(fat\ mass + lean\ mass)} \times 100$$

Body composition measurements were performed at baseline (one day prior to insulin supplementation) and after 28 days.

Transmission electron microscopy (TEM)

For TEM, the EDL was fixed in a 2% (w/v) glutaraldehyde solution with 0.1 M sodium cacodylate, pH 7.4. The samples were then fixed in 1% (w/v) osmium tetroxide (OsO_4) for 1 h and dehydrated sequentially in acetone (25%, 50%, 75% and 100% (v/v)) twice over 24 h. The EDL was then embedded in 100% resin at 60 °C for 24 h. Ultrathin sections (70 nm) were cut, stained with 2% (v/v) aqueous uranyl acetate and lead citrate and examined on a JEOL TEM-1400 transmission electron microscope (Electron Microscope Unit, Mark Wainwright Analytical Centre, UNSW Sydney, Australia). Electron micrographs were taken at 10,000 - 100,000× magnification. Semi-quantitative scoring of mitochondrial quality was performed as previously described[21], with mitochondria categorized as normal, elongated, or disintegrated (Supplementary Figure 1).

Second Harmonic Generation imaging

Single EDL muscle fibres were fixed with 4% (v/v) paraformaldehyde and analysed using a TimScope II multiphoton microscope (LaVision BioTec, Bielefeld, Germany) with a mode-locked ps-pulsed Ti:Sa laser source (Chameleon Vision II, Coherent, Scientifica, Uckfield, UK), tuned to 810 nm to excite the Second Harmonic Generation (SHG) signal of myosin at an average laser power of 16 mW. Pulse duration was centred around 2 ps with a repetition frequency of 80 MHz. The sample was placed between two opposing water immersion objectives, one (40×/1.1/UV-VIS-IR/WD 0.62; Zeiss, Germany) for the excitation beam path and a W Plan-Apochromat lens (20×/1.0/(UV)VIS-IR/WD 1.88/DIC M27 75 mm; Zeiss) for the transmission beam path. A 405/20 band pass (Chroma) filter was inserted to filter for the myosin transmission signal of ~400 nm in forward-scattered direction. The transmission signal was detected by a transmission photo multiplier tube (PMT, H7422-40, Hamamatsu Photonics, Shizuoka, Japan).

Exercise protocol

For exercise capacity studies, mice were trained for three consecutive days (20 min/day) on a rodent treadmill (Exer 3/6 Treadmill, Columbus Instruments, Columbus, OH). On the first day, the treadmill speed was set to a warm-up period of running at 5 m/min for 10 min. On the following training days, the initial speed was increased by 1 m/min every min to 15 m/min after the 10 min warm-up period. The mice were then rested for 2 days before the experimental run. On the day of the treadmill studies, mice were run on the treadmill at an initial speed of 15 m/min after the 10 min warm-up period. After 30 min, the speed was increased by 1 m/min every 15 min. Running was confirmed visually, and mice that stopped running were gently pushed back onto the belt with a paper towel. The mice were run to exhaustion, as judged by refusal to remain on the treadmill belt. Exercise capacity was calculated as performed work using the following formula:

$$Work\ (J) = body\ weight\ (kg) \times speed\ (m/min) \times time\ (\mathrm{min}) \times 9.8\ (\frac{J}{kg \times min})$$

Exercise studies were performed at baseline (2 days prior to insulin supplementation, 1 day prior to EchoMRI) and 28 days after insulin pump implantation.

Single muscle fibre biomechanical properties

Muscle strength was assessed by contractile performance assessment. Single fibre segments were manually isolated from dissected EDL muscles and myofibrillar Ca^{2+} sensitivity of the contractile apparatus quantified using the *MyoRobot* automated biomechatronics platform as described previously[22, 23]. Five to ten single fibres were analysed for each individual muscle sample. After mild membrane permeabilization with saponin, Ca^{2+}-induced force responses were induced by sequentially bathing the skinned fibre in solutions with increasing Ca^{2+} concentrations using defined mixtures of Ca^{2+} free and Ca^{2+}-saturated internal solutions[22, 23]. After reconstructing a sigmoidal curve from the steady-state force levels over each pCa, the pCa_{50} was extracted. To control for variability in baseline readings across experiments, values were normalised to maximum force.

Statistical analyses

Exercise and metabolic data are presented as the median of individual values. Data were assessed for normality using the D'Agostino-Pearson normality test. Differences between the groups were compared using the Wilcoxon test for paired analyses and Mann-Whitney U test for unpaired analyses or one way ANOVA, as appropriate. A value of $p < 0.05$ was considered to be statistically significant. GraphPad Prism software (version 9) was used for statistical analyses.

Results

Insulin insufficiency regulates gene expression in skeletal muscle

To examine the molecular consequences of insufficient insulin on skeletal muscle gene expression, we performed RNA sequencing on pooled EDL samples. A total of 59 transcripts were differentially regulated between the fl/fl control mice and β-DKO mice that did not receive insulin supplementation (Figure 1A; Supplementary Table 1). Gene Ontology cellular component analysis identified significant differential expression of various components of the contractile apparatus and cytoskeleton (Figure 1B). Biological process analysis indicated significant alterations in pathways involved in contraction and movement (Figure 1C).

We next asked what impact insulin supplementation in β-DKO mice had on the expression of these transcripts. We used an insulin dosing regimen that restores plasma insulin levels to that of control mice in the fed state[15]. Principle component analysis demonstrated clustering of replicate samples, with insulin-supplemented β-DKO mice being more closely related to fl/fl control mice than to β-DKO mice that were treated with PBS (Figure 2A). In total, a significant difference in the expression of 33 transcripts between β-DKO mice treated with insulin versus PBS was observed (Figure 2B; Supplementary Table 2), with 21 of these transcripts being restored to levels similar to those observed in fl/fl control mice (Figure 2C). Insulin supplementation restored expression of transcripts that are critical for muscle function and homeostasis such as heat shock protein 1A (*Hspa1a*), myoglobin and several myosin subunits.

Skeletal muscle loss is corrected by insulin supplementation in β-DKO mice

Similar to our previous findings[15], a comparable increase in body weight over the treatment period was observed for all groups of mice ($p<0.05$ for all; Figure 3A-C). Whilst

lean body mass percentage significantly decreased over the pump implantation period in both fl/fl (p=0.019; Figure 3D) and β-DKO mice treated with PBS (p=0.023; Figure 3E), there was no significant change in lean body mass percentage in β-DKO mice treated with insulin (Figure 3F).

Insulin insufficiency in β-DKO mice drives ultrastructural changes in sarcomeric muscle integrity

SHG microscopy was applied to EDL muscle sections to visualise myofibrillar architecture in fibres in a label-free manner. This approach has been shown to provide a structural correlate to muscle fibre 'weakness' as a consequence of altered ultrastructural hierarchical order of myofibrils[24]. Qualitative analysis of muscle fibres from fl/fl mice demonstrated a hierarchic pattern with a clear distinction of regularly arranged sarcomeres, indicative or parallel aligned myofibrils (Figure 4A). In contrast, fibres from β-DKO mice that received PBS showed abnormalities such as loss of striation (Figure 4C, white arrow) and myofibrillar breaks (Figure 4C, red arrow). Fibre architecture was largely restored in insulin-treated β-DKO mice (Figure 4E).

Analyses of EDL muscle from control mice by TEM displayed an intact structure with a parallel register of myofibrils and a series of clearly organized sarcomeres with clear Z-lines (Figure 4B). In contrast, muscle from PBS-treated β-DKO mice had severely altered ultrastructure characterized by disorganized myofibrillar register and misaligned Z-lines (Figure 4D), confirming the findings from the SHG images. Further, vesicle-like structures were apparent along the Z-lines that protruded into the surrounding myofibrils (Figure 4D, black arrows). Significant restoration of normal ultrastructure was observed in β-DKO mice treated with insulin, with alignment of Z-lines and parallel myofibrillar organisation (Figure 4F), again, confirming the findings from the SHG method.

Insulin insufficiency decreases mitochondrial number and integrity

Muscle mitochondrial number was significantly decreased in PBS-treated β-DKO mice relative to fl/fl control mice (0.47±0.15 vs 0.63±0.28 per μm^2, respectively, $p<0.01$; Figure 4G). Whilst supplementation of β-DKO mice with insulin increased muscle mitochondrial content (0.56±0.22 per μm^2), this did not reach statistical significance (Figure 4G). To better understand the impact of insulin supplementation on mitochondria, mitochondria were characterised as 'Normal', 'Elongated' or 'Disintegrated' based on shape and membrane and cristae integrity (Supplementary Figure 1). In muscles isolated from the fl/fl mice, 100% of mitochondria appeared normal (Figure 4H). The proportion of normal mitochondria was significantly reduced in PBS treated β-DKO mice ($p<0.001$), with most mitochondria classified as elongated (60%) or disintegrated (20%). Insulin supplementation significantly improved mitochondrial quality (60% normal, 35% elongated, 5% disintegrated, $p<0.001$).

Insulin supplementation restores *in vivo* exercise capacity and single fibre myofibrillar Ca^{2+}-sensitivity in β-DKO mice

Prior to pump implantation, low intensity endurance running on a rodent treadmill revealed that exercise capacity was significantly lower in β-DKO mice compared to fl/fl controls (211.8±84.47 vs 366.9±110.7 J for β-DKO and fl/fl mice, respectively; $p=0.005$; Figure 5A). Significant age-related declines in exercise capacity were observed for both the fl/fl (366.9±110.7 vs 314.5±106.2 J, $p<0.01$) and PBS treated β-DKO (239.7±113.2 vs 183.7±94.7 J, $p<0.005$) groups 28 days post pump implantation. Insulin supplementation not only prevented the decline in running performance but significantly increased exercise capacity in β-DKO mice (187.3±42.7 vs 254.9±39.4 J, $p<0.005$).

In parallel, performance differences were also observed in the Ca^{2+}-sensitivity of the contractile apparatus at the single fibre level (Figure 5B). Graded Ca^{2+}-induced force

measurements performed in isolated EDL skinned fibres demonstrated significant calcium desensitisation in PBS treated β-DKO fibres compared to those from fl/fl control mice (pCa_{50} = 6.08±0.16 vs 6.18±0.13, respectively; $p<0.05$). Insulin supplementation corrected the calcium desensitization in β-DKO mice back to control levels (pCa_{50} = 6.19±0.13, $p<0.05$).

Discussion

A failure to maintain healthy muscle is a common clinical feature of diabetic skeletal muscle disease and myopathy in type 1 and type 2 diabetes. This condition is characterized by loss of muscle mass, weakness, and overall reduced physical capacity. Distinct changes in skeletal muscle ultrastructure, such as disruption of the fibrillar registry and morphological abnormalities in mitochondria have also been reported in patients with type 1 diabetes[9]. Moreover, accumulation of intracellular lipids has been linked to several pathological complications in skeletal muscle including alterations in insulin sensitivity and signalling. In turn, impaired skeletal muscle metabolism can drive the pathogenesis of insulin resistance and glucose intolerance in diabetes although the underlying mechanisms remain unclear[25]. As the underlying mechanisms responsible for the diminished muscle mass and performance in diabetes are not known, identification of pathophysiological mechanisms and regulation of key metabolic pathways in diabetic muscle will substantially advance current knowledge of the relationship between muscle function and diabetes. This study investigated the effect of β-cell dysfunction and insulin insufficiency on skeletal muscle performance, morphology, mitochondrial structure, and gene expression in mice.

The significant reduction in circulating insulin levels in the β-DKO mice relative to fl/fl controls resulted in a decrease in the number of myosin heavy chain IIx Myh1 transcript associated with fast twitch fibres which are the predominant constituents of EDL muscle in mice[26, 27]. Supplementation of β-DKO with insulin led to a significant normalisation of the expression

of several myoglobin heavy chain isoforms including Mhy1, Mhy4 and Mhy7 as well as myoglobin which plays a critical role in oxygen metabolism in muscle. In contrast, whilst Myh2 levels were decreased in the EDL of β-DKO mice relative to fl/fl control, insulin treatment did not reverse this. Insulin has previously been shown to acutely upregulate expression of IIx-associated myosin heavy chain proteins in human *vastus lateralis* muscle[28]. This shift from glycolytic to oxidative fibre types agrees with our earlier characterisation of β-DKO mice skeletal muscle, where we proposed a shift in metabolic substrates in *gastrocnemius* muscle due to insufficient circulating insulin levels[15]. In this study, whilst muscle glycogen phosphorylase was upregulated in β-DKO mice relative to fl/fl controls, indicating increased use of glycogen as fuel source, differential expression of other transcripts involved in these pathways was not observed. However, this study utilised EDL muscle, a fast-twitch glycolytic muscle rather than *gastrocnemius* which is a fast-twitch oxidative muscle, and this fact may account for the differences observed between these studies. Downregulation of heat shock protein 1A (Hsp70) was the largest identified transcript change between the fl/fl and β-DKO mice, with expression being restored by insulin treatment. Whilst it is well established that insulin induces expression of Hsp70[29], Hsp70 also regulates skeletal muscle insulin sensitivity [30] and is an important biomarker in contraction injury prevention[31]. As such, modulation of Hsp70 expression has attracted attention as a therapeutic target. Further, Hsp70 regulates FoxO signalling[32], which plays important roles in maintaining muscle energy homeostasis through the control of glycolytic and lipolytic flux, and mitochondrial metabolism[33], as well as regulating diabetes-related muscle atrophy[34].

This study found perturbation of skeletal muscle homeostasis in the β-DKO model was associated with decreased exercise capacity and alterations of muscle ultrastructure. This was qualitatively shown using two independent imaging techniques, label-free two-photon

SHG imaging and TEM. A prominent feature was a loss of regular striation pattern with disruptions in myofibrillar lattice. Although due to sample size this was only qualitatively assessed here, previous detailed analyses applying quantitative morphometry to single fibre ultrastructure and simultaneous force recordings in a dystrophic mouse model showed that aberrant myofibrillar alignment is directly correlated with weakness in a graded manner[24]. The reduced *in vivo* exercise capacity in β-DKO mice and restoration in insulin-treated animals was also reflected on the single fibre level with a desensitisation of the contractile apparatus in β-DKO mice compared with controls and full restoration following insulin treatment.

This study has implications for populations in which β-cell dysfunction can occur prior to insulin resistance[35], such as in patients with type 1 diabetes where loss of skeletal muscle function is more akin to accelerated aging[36]. It suggests that early therapeutic intervention may be the preferred course of treatment for these patients. Indeed, lower BMI and metformin have both been shown to lower the risk of sarcopenia in T2DM[37]. This is in contrast to inflammatory mediated cancer-related cachexia where functionality is maintained, and exercise mediated interventions are recommended[38].

Acknowledgements

DAAD – Universities Australia Co-operation Scheme #57443180 to OF and PP. The authors acknowledge the facilities and the scientific and technical assistance of the Electron Microscope Unit within the Mark Wainwright Analytical Centre at UNSW Sydney, and in particular the assistance of Mrs Natasha Kapoor-Kaushik.

References

1. Sartori R, Romanello V, Sandri M. Mechanisms of muscle atrophy and hypertrophy: implications in health and disease. Nat Commun. 2021;12:330. doi:10.1038/s41467-020-20123-1

2. Takahashi F, Hashimoto Y, Kaji A, Sakai R, Okamura T, Kitagawa N, et al. Sarcopenia Is Associated With a Risk of Mortality in People With Type 2 Diabetes Mellitus. Front Endocrinol (Lausanne). 2021;12:783363. doi:10.3389/fendo.2021.783363

3. Au PC, Li HL, Lee GK, Li GH, Chan M, Cheung BM, et al. Sarcopenia and mortality in cancer: A meta-analysis. Osteoporos Sarcopenia. 2021;7:S28-S33. doi:10.1016/j.afos.2021.03.002

4. von Haehling S, Garfias Macedo T, Valentova M, Anker MS, Ebner N, Bekfani T, et al. Muscle wasting as an independent predictor of survival in patients with chronic heart failure. J Cachexia Sarcopenia Muscle. 2020;11:1242-9. doi:10.1002/jcsm.12603

5. Maeda K, Akagi J. Muscle Mass Loss Is a Potential Predictor of 90-Day Mortality in Older Adults with Aspiration Pneumonia. J Am Geriatr Soc. 2017;65:e18-e22. doi:10.1111/jgs.14543

6. Metter EJ, Talbot LA, Schrager M, Conwit R. Skeletal muscle strength as a predictor of all-cause mortality in healthy men. J Gerontol A Biol Sci Med Sci. 2002;57:B359-65. doi:10.1093/gerona/57.10.b359

7. Ostler JE, Maurya SK, Dials J, Roof SR, Devor ST, Ziolo MT, et al. Effects of insulin resistance on skeletal muscle growth and exercise capacity in type 2 diabetic mouse models. American journal of physiology Endocrinology and metabolism. 2014;306:E592-605. doi:10.1152/ajpendo.00277.2013

8. Egan B, Zierath JR. Exercise metabolism and the molecular regulation of skeletal muscle adaptation. Cell metabolism. 2013;17:162-84. doi:10.1016/j.cmet.2012.12.012

9. Krause MP, Riddell MC, Hawke TJ. Effects of type 1 diabetes mellitus on skeletal muscle: clinical observations and physiological mechanisms. Pediatr Diabetes. 2011;12:345-64. doi:10.1111/j.1399-5448.2010.00699.x

10. Russell ST, Rajani S, Dhadda RS, Tisdale MJ. Mechanism of induction of muscle protein loss by hyperglycaemia. Experimental cell research. 2009;315:16-25. doi:10.1016/j.yexcr.2008.10.002

11. Perry BD, Caldow MK, Brennan-Speranza TC, Sbaraglia M, Jerums G, Garnham A, et al. Muscle atrophy in patients with Type 2 Diabetes Mellitus: roles of inflammatory pathways, physical activity and exercise. Exercise immunology review. 2016;22:94-109.

12. O'Neill ED, Wilding JP, Kahn CR, Van Remmen H, McArdle A, Jackson MJ, et al. Absence of insulin signalling in skeletal muscle is associated with reduced muscle mass and function: evidence for decreased protein synthesis and not increased degradation. Age (Dordr). 2010;32:209-22. doi:10.1007/s11357-009-9125-0

13. Templeman NM, Mehran AE, Johnson JD. Hyper-Variability in Circulating Insulin, High Fat Feeding Outcomes, and Effects of Reducing Ins2 Dosage in Male Ins1-Null Mice in a Specific Pathogen-Free Facility. PLoS One. 2016;11:e0153280. doi:10.1371/journal.pone.0153280

14. Templeman NM, Flibotte S, Chik JHL, Sinha S, Lim GE, Foster LJ, et al. Reduced Circulating Insulin Enhances Insulin Sensitivity in Old Mice and Extends Lifespan. Cell Rep. 2017;20:451-63. doi:10.1016/j.celrep.2017.06.048

15. Cochran BJ, Hou L, Manavalan AP, Moore BM, Tabet F, Sultana A, et al. Impact of Perturbed Pancreatic beta-Cell Cholesterol Homeostasis on Adipose Tissue and Skeletal Muscle Metabolism. Diabetes. 2016;65:3610-20. doi:10.2337/db16-0668

16. Patro R, Duggal G, Love MI, Irizarry RA, Kingsford C. Salmon provides fast and bias-aware quantification of transcript expression. Nat Methods. 2017;14:417-9. doi:10.1038/nmeth.4197

17. Robinson MD, McCarthy DJ, Smyth GK. edgeR: a Bioconductor package for differential expression analysis of digital gene expression data. Bioinformatics. 2010;26:139-40. doi:10.1093/bioinformatics/btp616

18. Risso D, Schwartz K, Sherlock G, Dudoit S. GC-content normalization for RNA-Seq data. BMC Bioinformatics. 2011;12:480. doi:10.1186/1471-2105-12-480

19. Risso D, Ngai J, Speed TP, Dudoit S. Normalization of RNA-seq data using factor analysis of control genes or samples. Nat Biotechnol. 2014;32:896-902. doi:10.1038/nbt.2931

20. Kaldunski ML, Smith JR, Hayman GT, Brodie K, De Pons JL, Demos WM, et al. The Rat Genome Database (RGD) facilitates genomic and phenotypic data integration across multiple species for biomedical research. Mamm Genome. 2022;33:66-80. doi:10.1007/s00335-021-09932-x

21. Shum AM, Mahendradatta T, Taylor RJ, Painter AB, Moore MM, Tsoli M, et al. Disruption of MEF2C signaling and loss of sarcomeric and mitochondrial integrity in cancer-induced skeletal muscle wasting. Aging (Albany NY). 2012;4:133-43. doi:10.18632/aging.100436

22. Haug M, Reischl B, Prolss G, Pollmann C, Buckert T, Keidel C, et al. The MyoRobot: A novel automated biomechatronics system to assess voltage/Ca(2+) biosensors and active/passive biomechanics in muscle and biomaterials. Biosens Bioelectron. 2018;102:589-99. doi:10.1016/j.bios.2017.12.003

23. Haug M, Meyer C, Reischl B, Prolss G, Nubler S, Schurmann S, et al. MyoRobot 2.0: An advanced biomechatronics platform for automated, environmentally controlled skeletal muscle single fiber biomechanics assessment employing inbuilt real-time optical imaging. Biosens Bioelectron. 2019;138:111284. doi:10.1016/j.bios.2019.04.052

24. Schneidereit D, Nubler S, Prolss G, Reischl B, Schurmann S, Muller OJ, et al. Optical prediction of single muscle fiber force production using a combined biomechatronics and

second harmonic generation imaging approach. Light Sci Appl. 2018;7:79. doi:10.1038/s41377-018-0080-3

25. Meng ZX, Tao W, Sun J, Wang Q, Mi L, Lin JD. Uncoupling Exercise Bioenergetics From Systemic Metabolic Homeostasis by Conditional Inactivation of Baf60 in Skeletal Muscle. Diabetes. 2018;67:85-97. doi:10.2337/db17-0367

26. Friedrich O, Weber C, von Wegner F, Chamberlain JS, Fink RH. Unloaded speed of shortening in voltage-clamped intact skeletal muscle fibers from wt, mdx, and transgenic minidystrophin mice using a novel high-speed acquisition system. Biophys J. 2008;94:4751-65. doi:10.1529/biophysj.107.126557

27. Toth MJ, Palmer BM, LeWinter MM. Effect of heart failure on skeletal muscle myofibrillar protein content, isoform expression and calcium sensitivity. Int J Cardiol. 2006;107:211-9. doi:10.1016/j.ijcard.2005.03.024

28. Houmard JA, O'Neill DS, Zheng D, Hickey MS, Dohm GL. Impact of hyperinsulinemia on myosin heavy chain gene regulation. J Appl Physiol (1985). 1999;86:1828-32. doi:10.1152/jappl.1999.86.6.1828

29. Ting LP, Tu CL, Chou CK. Insulin-induced expression of human heat-shock protein gene hsp70. J Biol Chem. 1989;264:3404-8.

30. Senf SM. Skeletal muscle heat shock protein 70: diverse functions and therapeutic potential for wasting disorders. Front Physiol. 2013;4:330. doi:10.3389/fphys.2013.00330

31. Li Q, Luo Z. Identification of Candidate Genes for Skeletal Muscle Injury Prevention in Two Different Types. J Comput Biol. 2019;26:1080-9. doi:10.1089/cmb.2019.0022

32. Senf SM, Dodd SL, Judge AR. FOXO signaling is required for disuse muscle atrophy and is directly regulated by Hsp70. Am J Physiol Cell Physiol. 2010;298:C38-45. doi:10.1152/ajpcell.00315.2009

33. Sanchez AM, Candau RB, Bernardi H. FoxO transcription factors: their roles in the maintenance of skeletal muscle homeostasis. Cell Mol Life Sci. 2014;71:1657-71. doi:10.1007/s00018-013-1513-z

34. O'Neill BT, Bhardwaj G, Penniman CM, Krumpoch MT, Suarez Beltran PA, Klaus K, et al. FoxO Transcription Factors Are Critical Regulators of Diabetes-Related Muscle Atrophy. Diabetes. 2019;68:556-70. doi:10.2337/db18-0416

35. Ahlqvist E, Storm P, Karajamaki A, Martinell M, Dorkhan M, Carlsson A, et al. Novel subgroups of adult-onset diabetes and their association with outcomes: a data-driven cluster analysis of six variables. Lancet Diabetes Endocrinol. 2018;6:361-9. doi:10.1016/S2213-8587(18)30051-2

36. Monaco CMF, Gingrich MA, Hawke TJ. Considering Type 1 Diabetes as a Form of Accelerated Muscle Aging. Exerc Sport Sci Rev. 2019;47:98-107. doi:10.1249/JES.0000000000000184

37. Weber MA, Krakowski-Roosen H, Schroder L, Kinscherf R, Krix M, Kopp-Schneider A, et al. Morphology, metabolism, microcirculation, and strength of skeletal muscles in cancer-related cachexia. Acta Oncol. 2009;48:116-24. doi:10.1080/02841860802130001

38. Ai Y, Xu R, Liu L. The prevalence and risk factors of sarcopenia in patients with type 2 diabetes mellitus: a systematic review and meta-analysis. Diabetol Metab Syndr. 2021;13:93. doi:10.1186/s13098-021-00707-7

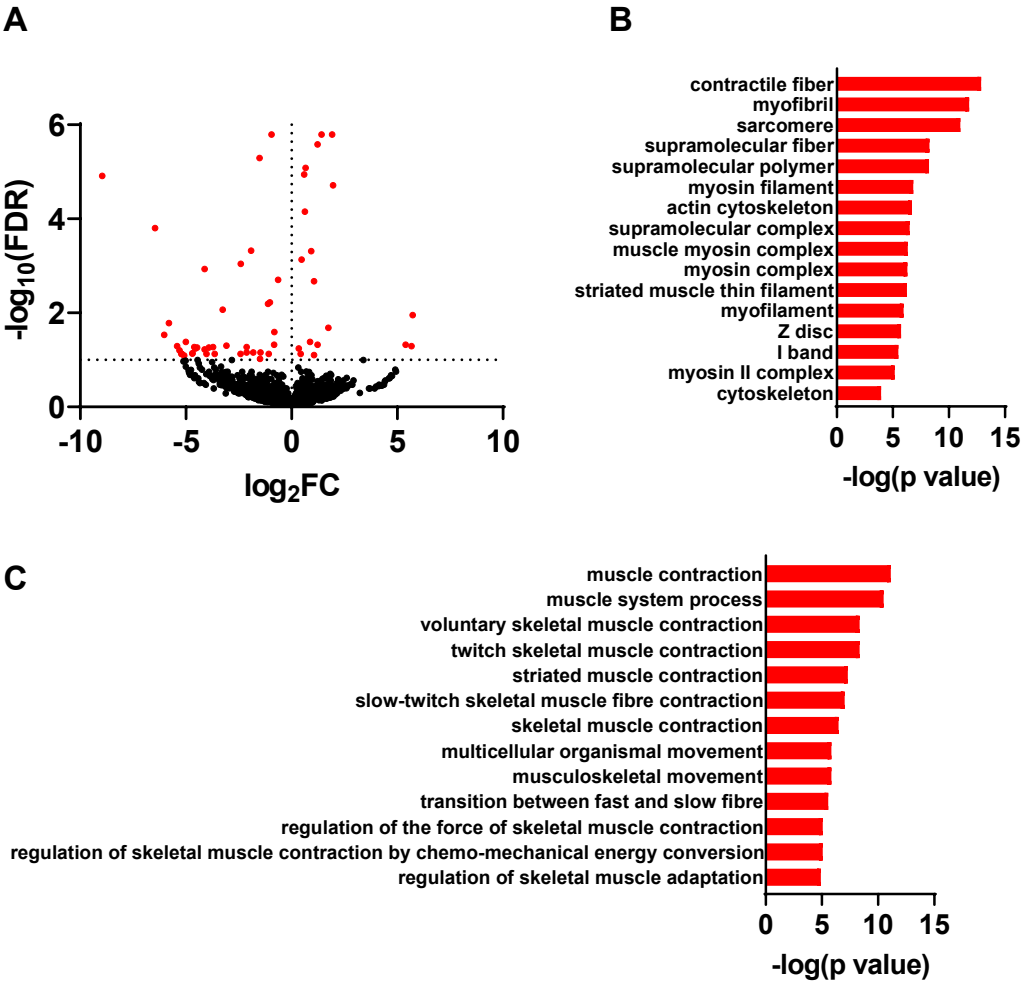

Figure 1: Insulin insufficiency results in decreased expression of transcripts involved in skeletal muscle structure and function. Bulk RNA sequencing was conducted on isolated EDL muscles from control fl/fl and PBS treated β-DKO mice. **(A)** Volcano plot of differentially expressed transcripts between fl/fl and PBS β-DKO mice. (**B**) Gene Ontology cellular component and (**C**) biological process results obtained using the Mouse Portal of the Rat Genome Database[20].

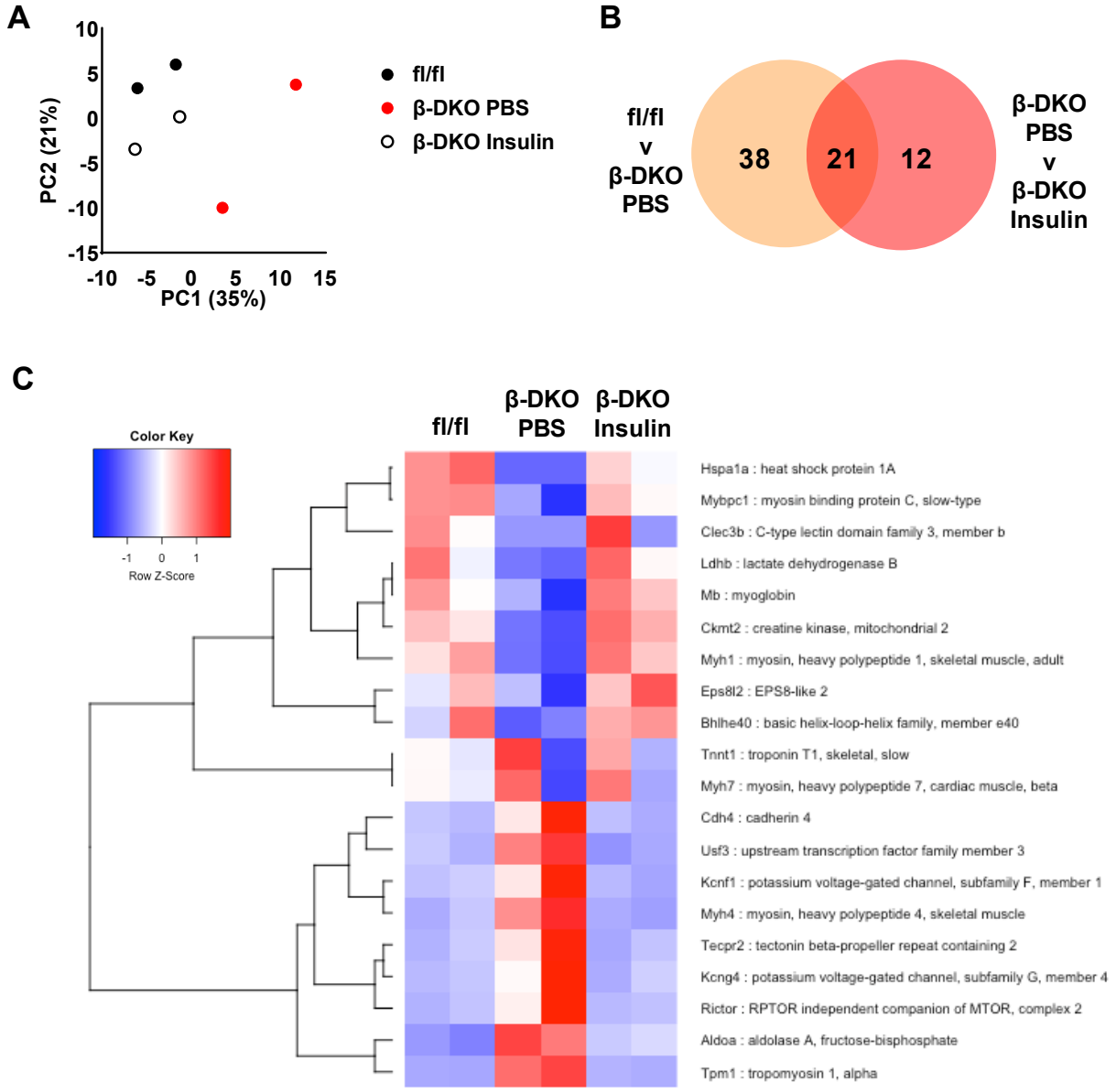

Figure 2: Insulin supplementation normalised the altered expression of skeletal muscle transcripts in β-DKO mice. (**A**) Principal component analysis of sequenced RNA transcripts from fl/fl control (black dots) and β-DKO mice treated with PBS (red dots) or insulin (white dots). (**B**) Of the 59 differentially expressed transcripts between fl/fl control and PBS treated β-DKO mice, 21 were normalised by in the insulin treated β-DKO mice. (**C**) Heat map and clustering analysis of the 21 transcripts normalised by insulin treatment.

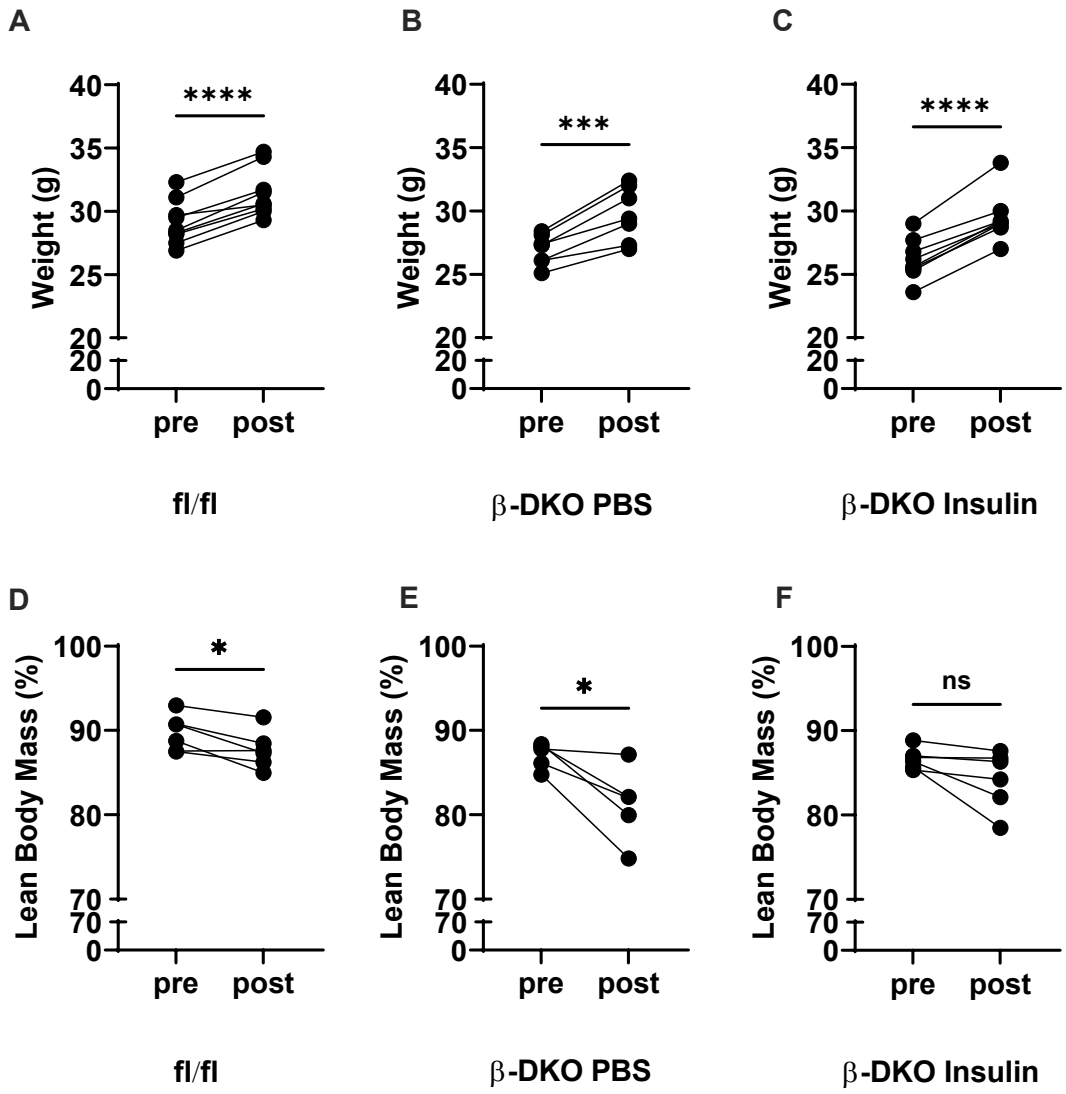

Figure 3. Insulin supplementation did not alter body weight but inhibited age-related lean body mass loss. Mice were weighed at baseline (pre) and 28 days after pump insertion (post). Body weight of (**A**) control fl/fl and β-DKO mice treated with (**B**) PBS or (**C**) insulin-containing pumps. Lean body mass of (**D**) control fl/fl and β-DKO mice treated with (**E**) PBS or (**F**) insulin containing pumps were determined by EchoMRI. *$p<0.05$, ***$p<0.005$, ns = not significant.

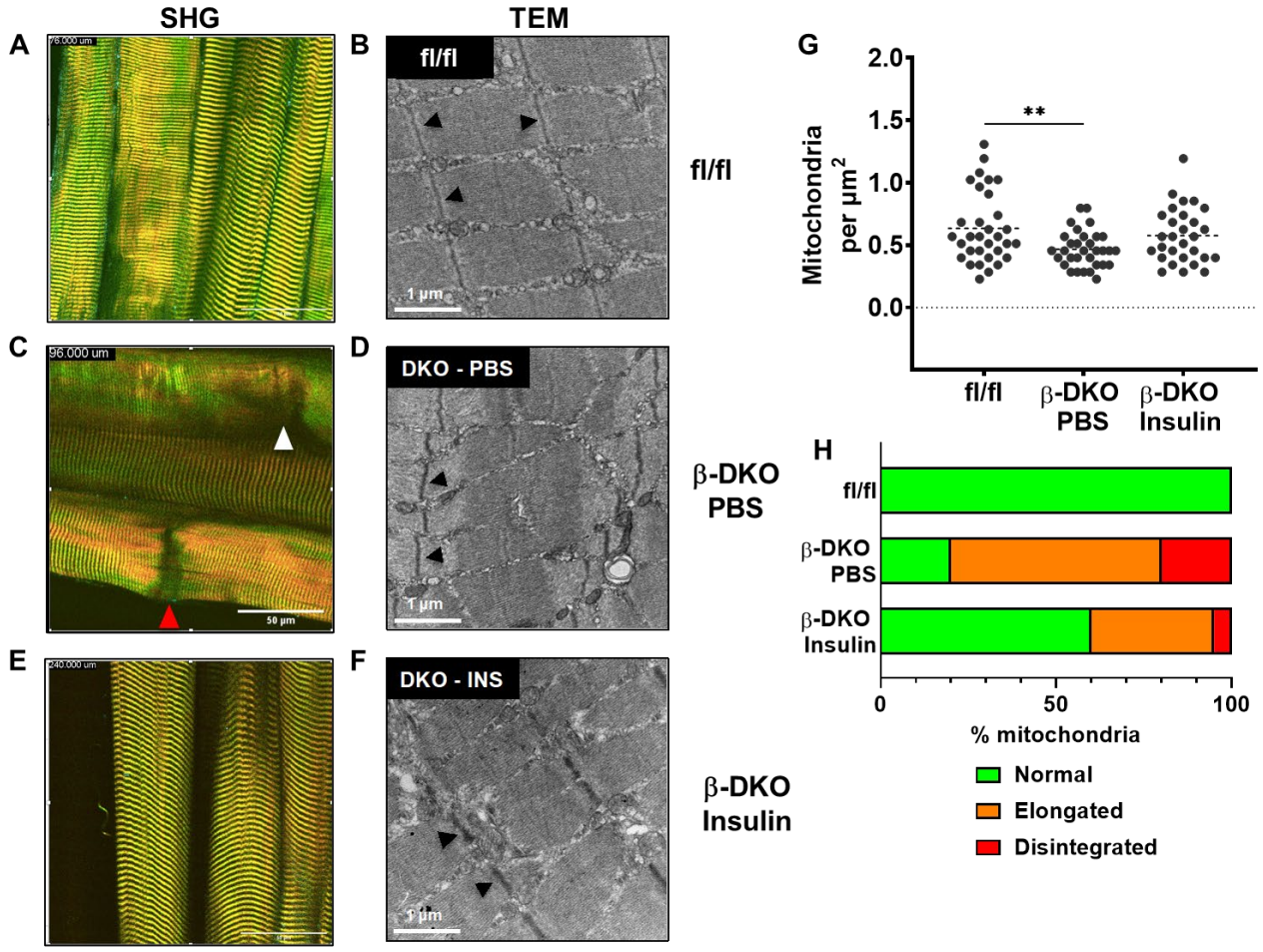

Figure 4. Insulin supplementation restores muscle ultrastructure and mitochondrial morphology. Representative Second Harmonic Generation (SHG) and transmission electron microscopy (TEM) images of EDL muscle sections from (**A, B**) fl/fl control and β-DKO mice treated with (**C, D**) PBS or (**E, F**) insulin. Loss of fibre striation and myofibrillar breaks are indicted by white and red arrows, respectively. Fibre registry and Z-line alignment (black arrowheads) were notably disrupted in the β-DKO PBS mice, and partially restored by insulin treatment. Quantification of mitochondrial (**G**) number and (**H**) quality obtained from multiple fields of view (n=7-10) for 3 animals per group. Dashed lines represent means. **p<0.01.

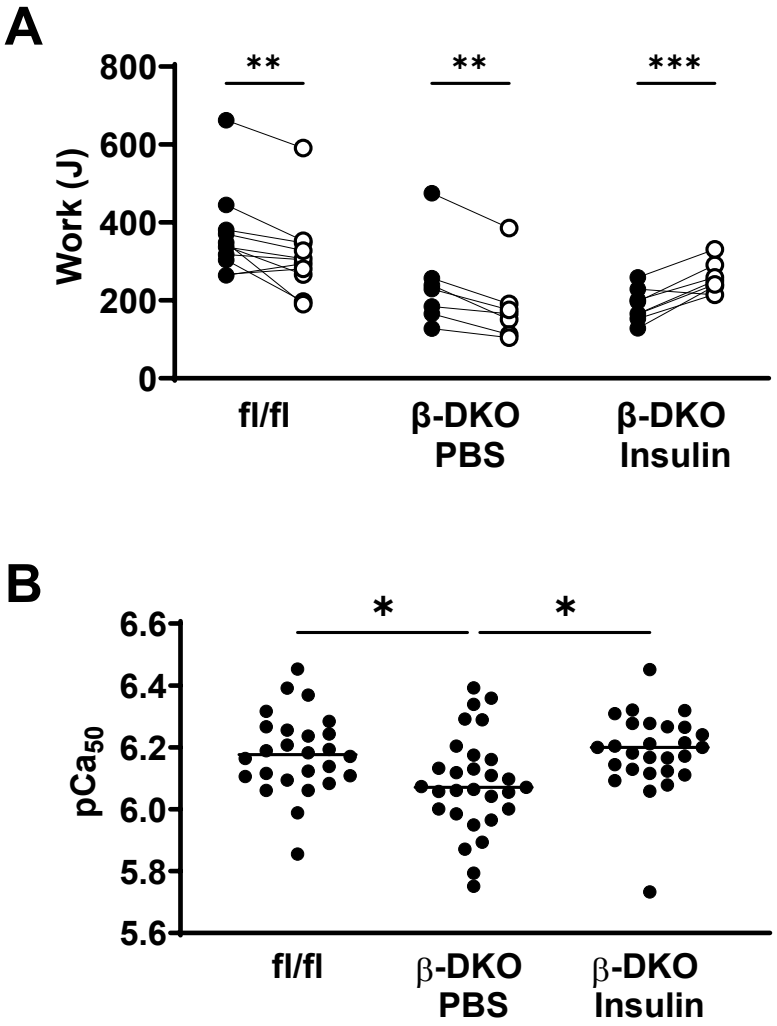

Figure 5. Insulin treatment improves exercise capacity and muscle strength in β-DKO mice. (A) Individual running performance was assessed at baseline (black circles) and 28 days post (white circles) pump implantation in fl/fl control and β-DKO mice treated with PBS or insulin. (**B**) Ca^{2+} sensitivity of the contractile apparatus was assessed by subjecting single fibres from the *extensor digitorum longus* muscle to Ca^{2+}-graded force measurements and determining pCa_{50} values. Bars represent mean value. *p<0.05; **p<0.01, ***p<0.001.

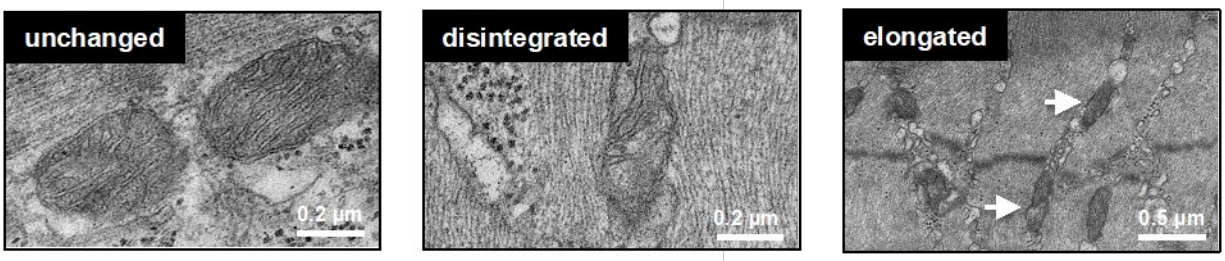

Supplementary Figure 1: Examples of mitochondria categories used for quantitative analysis of mitochondrial quality in EDL muscle by TEM.

Supplementary Table 1: Transcripts differentially expressed between control fl/fl mice and β-DKO mice treated with PBS. A false discovery rate (FDR) < 0.1 cut-off was used to identify transcripts with significantly altered expression.

	Fold change	False discovery rate
Expression increased in β-DKO vs fl/fl control		
fascin actin-bundling protein 2|Fscn2	53.17422	0.011257
phospholipase A2, group IVB (cytosolic)|Pla2g4b	51.05106	0.051346
syntaxin binding protein 3|Stxbp3	42.22384	0.048006
cadherin 4|Cdh4	3.892833	1.97E-05
RPTOR independent companion of MTOR, complex 2|Rictor	3.771738	1.63E-06
mab-21-like 1 (C. elegans)|Mab21l1	3.333985	0.020934
potassium voltage-gated channel, subfamily G, member 4|Kcng4	2.663953	1.63E-06
upstream transcription factor family member 3|Usf3	2.35029	2.64E-06
potassium voltage-gated channel, subfamily F, member 1|Kcnf1	2.348649	0.048006
S-adenosylmethionine decarboxylase 1|Amd1	2.086871	0.079413
tectonin beta-propeller repeat containing 2|Tecpr2	2.083586	0.002116
high mobility group AT-hook 2|Hmga2	1.902717	0.000487
serine/threonine kinase 11|Stk11	1.83706	0.041278
myosin, heavy polypeptide 4, skeletal muscle|Myh4	1.582213	8.36E-06
actinin alpha 3|Actn3	1.539407	7.1E-05
tropomyosin 1, alpha|Tpm1	1.507017	1.14E-05
creatine kinase, muscle|Ckm	1.38831	0.000742
muscle glycogen phosphorylase|Pygm	1.349962	0.074726
aldolase A, fructose-bisphosphate|Aldoa	1.267484	0.058175
Expression decreased in β-DKO vs fl/fl control		
myosin, heavy polypeptide 1, skeletal muscle, adult|Myh1	1.559699	0.001992
glutathione synthetase|Gss	1.762453	0.02551
creatine kinase, mitochondrial 2|Ckmt2	1.776419	0.048006
myosin binding protein C, slow-type|Mybpc1	1.927011	1.63E-06
actinin alpha 2|Actn2	2.042271	0.006034
protein tyrosine phosphatase, receptor type, Q|Ptprq	2.124977	0.074726
myoglobin|Mb	2.171065	0.006388
EPS8-like 2|Eps8l2	2.766763	0.068619
E74-like factor 1|Elf1	2.816357	0.094722
myosin, heavy polypeptide 2, skeletal muscle, adult|Myh2	2.851151	5.18E-06
spectrin repeat containing, nuclear envelope 1|Syne1	3.512969	0.068619
predicted gene 11127|Gm11127	3.762789	0.000473
leukocyte receptor cluster (LRC) member 8|Leng8	4.360866	0.068619
lactate dehydrogenase B|Ldhb	4.362688	0.053787
ankyrin repeat and zinc finger domain containing 1|Ankzf1	5.299245	0.000905
Ras association (RalGDS/AF-6) domain family (N-terminal) member 8|Rassf8	5.336577	0.074726
troponin T1, skeletal, slow|Tnnt1	8.473621	0.049599
myosin, heavy polypeptide 7, cardiac muscle, beta|Myh7	9.622791	0.008427

neurexophilin and PC-esterase domain family, member 2|Nxpe2	12.42636	0.074726
biorientation of chromosomes in cell division 1|Bod1	13.11243	0.053787
predicted gene 4631|Gm14430; Gm4631	15.0583	0.054729
collagen, type I, alpha 1|Col1a1	16.35819	0.074726
predicted gene 906|Gm906	17.33313	0.001178
acyl-CoA synthetase long-chain family member 1|Acsl1	17.36458	0.060152
ribosomal protein S27, retrogene|Rps27rt	22.1178	0.054729
neuron derived neurotrophic factor|Nenf	23.50486	0.058175
giant axonal neuropathy|Gan	24.31692	0.053787
UBX domain protein 2A|Ubxn2a	25.80869	0.07179
tripartite motif-containing 43B|Trim43b	25.80869	0.07179
basic helix-loop-helix family, member e40|Bhlhe40	32.1067	0.041278
syntaxin 12|Stx12	33.97626	0.081574
family with sequence similarity 32, member A|Fam32a	36.9039	0.074726
presequence translocase-asssociated motor 16 homolog (S. cerevisiae)|Pam16	36.9039	0.074726
discs large MAGUK scaffold protein 1|Dlg1	36.9039	0.074726
peptidase inhibitor 16|Pi16	39.67304	0.063279
C-type lectin domain family 3, member b|Clec3b	42.76348	0.051346
prolyl 3-hydroxylase 1|P3h1	56.09781	0.01675
family with sequence similarity 98, member C|Fam98c	65.27687	0.029358
heat shock protein 1A|Hspa1a	88.14633	0.00016
predicted gene, 28042|-	499.6327	1.22E-05

Supplementary Table 2: Transcripts differentially expressed between β-DKO mice treated with PBS and insulin. A false discovery rate (FDR) < 0.1 cut-off was used to identify transcripts with significantly altered expression.

	Fold change	False discovery rate
Expression increased in β-DKO Ins vs β-DKO PBS		
heat shock protein 1A|Hspa1a	50.71743	0.021103
3-hydroxybutyrate dehydrogenase, type 1|Bdh1	43.07484	0.056071
C-type lectin domain family 3, member b|Clec3b	32.13608	0.004231
myocilin|Myoc	27.74192	0.061562
basic helix-loop-helix family, member e40|Bhlhe40	24.25457	0.040214
predicted gene 4631|Gm14430; Gm4631	21.51709	0.041108
myosin, heavy polypeptide 7, cardiac muscle, beta|Myh7	15.1365	0.000123
troponin T1, skeletal, slow|Tnnt1	9.367069	0.010102
myosin, light chain 12A, regulatory, non-sarcomeric|Myl12a	9.216469	0.001703
somatostatin receptor 3|Sstr3	8.327212	0.056071
lactate dehydrogenase B|Ldhb	4.353275	0.080173
microtubule-associated protein 1 A|Map1a	4.070883	0.055235
EPS8-like 2|Eps8l2	3.439704	0.003969
myoglobin|Mb	2.250541	0.000735
creatine kinase, mitochondrial 2|Ckmt2	1.961628	0.011665
myosin binding protein C, slow-type|Mybpc1	1.599328	0.084026
myosin, heavy polypeptide 1, skeletal muscle, adult|Myh1	1.594162	0.009398
mitochondrially encoded NADH dehydrogenase 2|ND2	1.396794	0.017172
mitochondrially encoded cytochrome c oxidase III|COX3	1.197349	0.09742
Expression decreased in β-DKO Ins vs β-DKO PBS		
aldolase A, fructose-bisphosphate|Aldoa	1.209698	0.09742
ryanodine receptor 1, skeletal muscle|Ryr1	1.287901	0.055235
myosin binding protein C, fast-type|Mybpc2	1.417734	0.008806
dual specificity phosphatase 1|Dusp1	1.439174	0.080173
tropomyosin 1, alpha|Tpm1	1.511536	9.97E-07
myosin, heavy polypeptide 4, skeletal muscle|Myh4	1.697096	4.00E-21
frizzled class receptor 7|Fzd7	1.983316	0.000208
tectonin beta-propeller repeat containing 2|Tecpr2	2.165953	0.007169
potassium voltage-gated channel, subfamily G, member 4|Kcng4	2.625393	0.010772
potassium voltage-gated channel, subfamily F, member 1|Kcnf1	2.877588	0.015407
upstream transcription factor family member 3|Usf3	2.961892	5.16E-09
RPTOR independent companion of MTOR, complex 2|Rictor	3.522655	1.16E-05
cadherin 4|Cdh4	4.737905	3.12E-05
Myosin regulatory light chain 12B|-	13.11259	0.056071
aldolase A, fructose-bisphosphate|Aldoa	1.209698	0.09742
ryanodine receptor 1, skeletal muscle|Ryr1	1.287901	0.055235
myosin binding protein C, fast-type|Mybpc2	1.417734	0.008806
dual specificity phosphatase 1|Dusp1	1.439174	0.080173
tropomyosin 1, alpha|Tpm1	1.511536	9.97E-07

myosin, heavy polypeptide 4, skeletal muscle|Myh4	1.697096	4.00E-21
frizzled class receptor 7|Fzd7	1.983316	0.000208
tectonin beta-propeller repeat containing 2|Tecpr2	2.165953	0.007169
potassium voltage-gated channel, subfamily G, member 4|Kcng4	2.625393	0.010772
potassium voltage-gated channel, subfamily F, member 1|Kcnf1	2.877588	0.015407
upstream transcription factor family member 3|Usf3	2.961892	5.16E-09
RPTOR independent companion of MTOR, complex 2|Rictor	3.522655	1.16E-05
cadherin 4|Cdh4	4.737905	3.12E-05
Myosin regulatory light chain 12B|-	13.11259	0.056071